PHYSICAL REVIEW LETTERS

Kinetic Turbulence in Relativistic Plasma:
From Thermal Bath to Nonthermal Continuum

Vladimir Zhdankin,[1,*] Gregory R. Werner,[2] Dmitri A. Uzdensky,[2,3] and Mitchell C. Begelman[1,4]

[1]*JILA, University of Colorado and NIST, 440 UCB, Boulder, Colorado 80309, USA*
[2]*Center for Integrated Plasma Studies, Physics Department, University of Colorado, 390 UCB, Boulder, Colorado 80309, USA*
[3]*Institute for Advanced Study, Princeton, New Jersey 08540, USA*
[4]*Department of Astrophysical and Planetary Sciences, 391 UCB, Boulder, Colorado 80309, USA*

We present results from particle-in-cell simulations of driven turbulence in magnetized, collisionless, and relativistic pair plasmas. We find that the fluctuations are consistent with the classical $k_\perp^{-5/3}$ magnetic energy spectrum at fluid scales and a steeper $k_\perp^{-4}$ spectrum at sub-Larmor scales, where $k_\perp$ is the wave vector perpendicular to the mean field. We demonstrate the development of a nonthermal, power-law particle energy distribution $f(E) \sim E^{-\alpha}$, with an index α that decreases with increasing magnetization and increases with an increasing system size (relative to the characteristic Larmor radius). Our simulations indicate that turbulence can be a viable source of energetic particles in high-energy astrophysical systems, such as pulsar wind nebulae, if scalings asymptotically become insensitive to the system size.

Introduction.—Nonthermal energetic particles are a common ingredient in high-energy astrophysics, being responsible for observable broadband radiation spectra. However, their origin is often poorly constrained. It is now widely accepted that nonthermal particle acceleration can be a consequence of collisionless plasma physics. In particular, it was demonstrated that relativistic magnetic reconnection [1–3] and collisionless shocks [4,5] can both efficiently energize a population of nonthermal particles with a power-law energy distribution. Since these two mechanisms require specific large-scale configurations to initiate, however, it is unclear whether they are sufficiently versatile to explain all observations.

A third route to particle acceleration, which may be both versatile and ubiquitous, is turbulence in collisionless plasmas. Turbulence is often inevitable in astrophysical flows due to the large separation between driving scales and dissipative scales, making it an attractive possible source of energetic particles. In particular, turbulence may power nonthermal synchrotron and inverse Compton radiation in systems such as pulsar wind nebulae, coronae of accreting objects, and jets. Furthermore, intermittent dissipative structures may naturally explain impulsive flares observed in some of these systems, including GeV flares in the Crab Nebula [6,7].

Turbulent particle acceleration can be associated with a number of acceleration mechanisms, which are not necessarily independent from those in shocks and magnetic reconnection. Indeed, large-scale turbulence may intermittently accelerate particles through first-order Fermi acceleration in self-consistently formed shocks and reconnection sites (e.g., [8–11]), while small-scale, instability-driven turbulence is essential for Fermi acceleration in shocks and reconnection [12,13]. Particles can also be stochastically accelerated via wave-particle interactions, generally leading to second-order Fermi acceleration (e.g., [14–18]). However, it remains largely unestablished under what circumstances the turbulent cascade can efficiently accelerate particles toward a robust nonthermal particle energy distribution.

In this Letter, we utilize particle-in-cell (PIC) simulations to demonstrate that kinetic turbulence in collisionless, relativistically hot pair plasmas can efficiently generate a nonthermal particle population from an initial thermal bath in closed systems of modest size. The simulations are driven to develop a classical large-scale magnetohydrodynamic (MHD) cascade that transitions into a kinetic cascade at sub-Larmor scales. The late-time particle distributions take the form of power laws that span a broad range of energies. For a fixed system size, these power-law distributions become harder with increasing magnetization (or decreasing plasma beta) and qualitatively resemble those previously seen in relativistic magnetic reconnection [2,3,19]. However, the distributions become steeper with increasing system size, indicating that asymptotic, system-size-independent scalings either have not yet been reached or do not exist.

Method.—Hydrodynamic and MHD simulations show that relativistic turbulence broadly resembles the nonrelativistic case [20–25] but can only describe acceleration in the test particle approximation (e.g., [26,27]). In this work, we apply kinetic PIC simulations, which, for hot pair plasmas, can obtain a comparable inertial range [28] while self-consistently describing particle acceleration. Previously, PIC simulations were applied to show the emergence of nonthermal features from decaying turbulence (e.g., [29–31]) and from the magnetorotational instability [32–34].

In our system, the magnetic field $\boldsymbol{B}(\boldsymbol{x}, t)$ and electric field $\boldsymbol{E}(\boldsymbol{x}, t)$ are evolved by Maxwell's equations, while the

electron and positron particles are evolved via the Lorentz force. The characteristic kinetic scales are the Larmor radius $\rho_e \equiv \bar{\gamma}mc^2/eB_{\mathrm{rms}}$ and plasma skin depth $d_e \equiv \sqrt{\bar{\gamma}mc^2/4\pi n_0 e^2}$, given the mean particle Lorentz factor $\bar{\gamma} \gg 1$, electron rest mass m, elementary charge e, speed of light c, mean total particle density n_0, and characteristic (rms) magnetic field B_{rms}. The two free dimensionless parameters (ignoring driving parameters) are the system size relative to Larmor radius L/ρ_e and nominal magnetization $\sigma \equiv B_{\mathrm{rms}}^2/4\pi n_0 \bar{\gamma}mc^2 = (d_e/\rho_e)^2$ (inversely proportional to plasma beta). We denote the initial values by $\sigma_0 \equiv \sigma(t=0)$ and $\rho_{e0} \equiv \rho_e(t=0)$.

We performed our simulations using the explicit electromagnetic PIC code Zeltron [35]. The domain is a periodic cubic box of size L^3 with uniform background magnetic field $\boldsymbol{B}_0 = B_0\hat{z}$. We initialize simulations with zero electromagnetic fluctuations ($\delta\boldsymbol{B} = \boldsymbol{E} = 0$) and particles with a uniform nondrifting Maxwell-Jüttner distribution [36] and ultrarelativistic mean Lorentz factor $\bar{\gamma}(t=0) \approx 300$. This stable thermal equilibrium is disrupted by external driving. To drive strong, critically balanced turbulence at large scales in a way that mimics energy transfer from a MHD cascade [37], we apply a fluctuating external current density $\boldsymbol{J}_{\mathrm{ext}}$ in the form of an oscillating Langevin antenna [38]. We drive $J_{\mathrm{ext},z}$ at eight modes, $\boldsymbol{k}_0 L/2\pi \in \{(1,0,\pm1),(0,1,\pm1),(-1,0,\pm1),(0,-1,\pm1)\}$, and each of $J_{\mathrm{ext},x}$ and $J_{\mathrm{ext},y}$ in four modes to enforce $\nabla \cdot \boldsymbol{J}_{\mathrm{ext}} = 0$. We choose driving frequency $\omega_0 = 0.6 \cdot 2\pi v_{A0}/\sqrt{3}L$ and decorrelation rate $\Gamma_0 = 0.5 \cdot 2\pi v_{A0}/\sqrt{3}L$, where $v_{A0} = c\sqrt{\sigma_0/(\sigma_0 + 4/3)}$ is the initial relativistic Alfvén velocity in our simulations [39,40]. We tune the driving amplitude such that rms fluctuations satisfy $\delta B_{\mathrm{rms}} \sim B_0$.

Since there is no energy sink in our numerical setup, injected energy will increase the fluid internal energy linearly in time at a heating rate (per unit volume) comparable to $\epsilon \sim B_0^2 c/8\pi L$. This heating will cause $\rho_e(t)$ to increase in time and $\sigma(t)$ to decrease in time, with the dimensionless parameter $\xi \equiv \sigma\rho_e/L$ being statistically constant in time. The parameter ξ can be expressed as $\xi = \mathcal{E}_{\mathrm{mag}}/\mathcal{E}_{\mathrm{max}}$, where $\mathcal{E}_{\mathrm{mag}} = B_{\mathrm{rms}}^2/8\pi n_0$ is the magnetic energy per particle and $\mathcal{E}_{\mathrm{max}} = LeB_{\mathrm{rms}}/2c$ is the maximum energy of particles for a given system size (i.e., with the Larmor radius equal to half the system size). All simulations with fixed ξ but varying σ nominally represent different stages of evolution for a single run. Fully developed turbulence begins after a few light crossing times (once the cascade reaches kinetic scales) and ends when the fluid inertial range is suppressed by heating ($\rho_e \sim L/2\pi$). A rough estimate for the duration of turbulence, assuming $\rho_e(t) \sim \rho_{e0} + t\epsilon/n_0 eB_{\mathrm{rms}}$, is $tc/L \sim L/2\pi\rho_{e0}\sigma_0 \sim 1/2\pi\xi(t=0)$.

Results.—We performed a series of simulations on lattices of N^3 cells with varying parameters σ_0 and L/ρ_{e0}. For simulations with $N \in \{256, 384, 512, 768, 1024\}$, we

chose a corresponding ratio of driving scale to initial Larmor radius no greater than $L/2\pi\rho_{e0} \in \{27.2, 40.7, 54.3, 81.5, 108.6\}$. For simulations with $N \leq 512$, we performed a full scan of $\sigma_0 \in \{0.25, 0.5, 1, 2, 4\}$; for $N = 768$, we did $\sigma_0 \in \{0.25, 0.5, 1, 2\}$; and for $N = 1024$, we did $\sigma_0 \in \{0.5, 2\}$. Unless otherwise noted, we describe results from our fiducial 768^3 simulation with $\sigma_0 = 0.25$ and $L/2\pi\rho_{e0} \approx 61.1$ (with $\sim 10^{11}$ particles). For all runs, we chose $\rho_{e0} \geq 1.5\Delta x$ (where Δx is the lattice cell size), at least 128 particles per cell [41], and a duration $\geq 10L/c$ (including $\sim 22L/c$ for the fiducial case); note that the Alfvén crossing time is longer than L/c and slowly increases in time. In most of our cases, the total energy (accounting for injection) is conserved to approximately 1% or better. We show a snapshot of $J_z/J_{z,\mathrm{rms}}$, the normalized electric current density along $\boldsymbol{B}_0$, in Fig. 1. The formation of intermittent current sheets, with thicknesses near the kinetic scale and lengths spanning a range of scales up to the driving scale, is evident, as previously seen in MHD turbulence (e.g., [42]) and in nonrelativistic kinetic turbulence (e.g., [28,43]).

We first show the evolution of the energy contributions in Fig. 2. We decompose total particle kinetic energy $E_{\mathrm{kin}}(t) = \int d^3x E_f(\boldsymbol{x}, t)$ into internal fluid energy
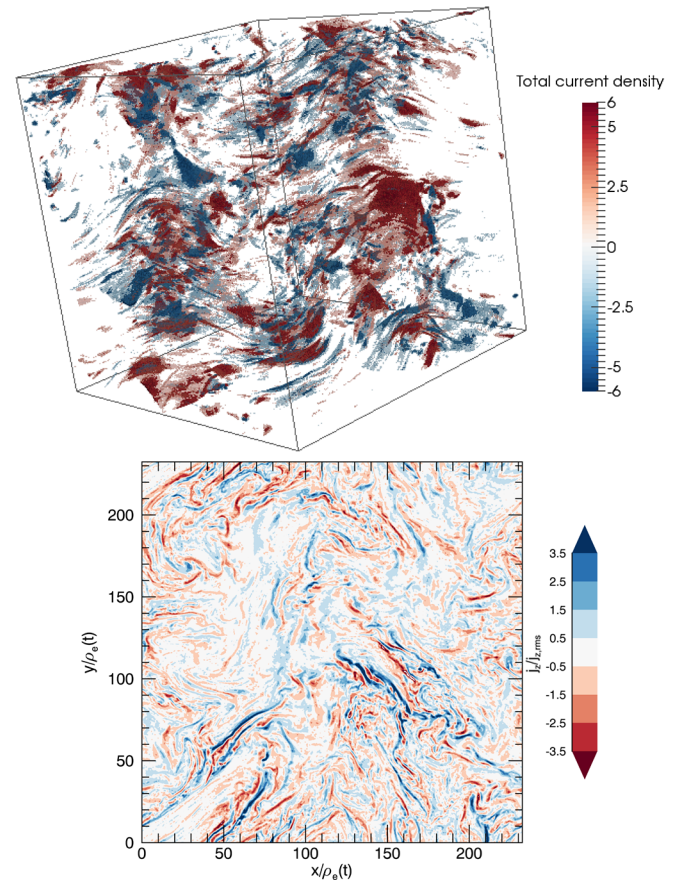

FIG. 1. 3D and 2D threshold plots of $J_z/J_{z,\mathrm{rms}}$ (normalized electric current density parallel to $\boldsymbol{B}_0$).
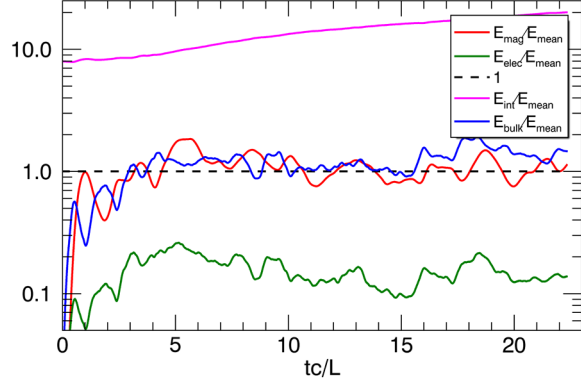
FIG. 2. Evolution of turbulent magnetic energy E_{mag} (red curve), electric energy E_{elec} (green curve), internal energy E_{int} (magenta curve), and bulk fluid energy E_{bulk} (blue curve), all normalized to background magnetic energy E_{mean} (black, dashed line).

$E_{\mathrm{int}}(t) = \int d^3x [E_f^2(\mathbf{x}, t) - p_f^2(\mathbf{x}, t)c^2]^{1/2}$ and bulk fluid kinetic energy $E_{\mathrm{bulk}}(t) = E_{\mathrm{kin}}(t) - E_{\mathrm{int}}(t)$, where $E_f(\mathbf{x}, t) = \int d^3p (m^2c^4 + p^2c^2)^{1/2} f(\mathbf{p}, \mathbf{x}, t)$ is the fluid energy density, $\mathbf{p}_f(\mathbf{x}, t) = \int d^3p \mathbf{p} f(\mathbf{p}, \mathbf{x}, t)$ is the fluid momentum density, and $f(\mathbf{p}, \mathbf{x}, t)$ is the particle distribution function at time t. Bulk fluid energy can also be expressed as $E_{\mathrm{bulk}}(t) = \int d^3x w^2(\mathbf{x}, t)$, where $\mathbf{w} \equiv \mathbf{p}_f c / [E_f + (E_f^2 - p_f^2 c^2)^{1/2}]^{1/2}$ is the fluid four-velocity weighted by an effective mass. We find that turbulent energy saturates after a few light crossing times. The turbulent magnetic energy $E_{\mathrm{mag}}(t) = \int d^3x [\delta \mathbf{B}(\mathbf{x}, t)]^2/8\pi$ and E_{bulk} come into equipartition with background magnetic energy $E_{\mathrm{mean}} = \int d^3x B_0^2/8\pi$, as dictated by our driving, while electric energy $E_{\mathrm{elec}}(t) = \int d^3x [\mathbf{E}(\mathbf{x}, t)]^2/8\pi$ is a few times smaller. For $\sigma_0 \leq 1$, turbulence energies are significantly below E_{int}, which sets fluid inertia, so turbulent motions are effectively nonrelativistic. To a good approximation, the internal energy increases linearly in time, as expected from a constant energy injection rate. For the fiducial case, ρ_e and d_e increase by less than a factor of 2 over the given duration.

We next consider Fourier power spectra for turbulent fluctuations. For simplicity, we consider the magnetic energy spectrum $E_{\mathrm{mag}}(\mathbf{k}) = |\tilde{\mathbf{B}}(\mathbf{k})|^2/8\pi$, electric energy spectrum $E_{\mathrm{elec}}(\mathbf{k}) = |\tilde{\mathbf{E}}(\mathbf{k})|^2/8\pi$, solenoidal fluid energy spectrum $E_{\mathrm{bulk,sol}}(\mathbf{k}) = |\hat{\mathbf{k}} \times \tilde{\mathbf{w}}(\mathbf{k})|^2$, and compressive fluid energy spectrum $E_{\mathrm{bulk,comp}}(\mathbf{k}) = |\hat{\mathbf{k}} \cdot \tilde{\mathbf{w}}(\mathbf{k})|^2$, where $\tilde{\mathbf{y}}(\mathbf{k})$ denotes the Fourier transform of $\mathbf{y}(\mathbf{x})$. The decomposition of fluid energy into solenoidal and compressive parts is customary in compressible turbulence (e.g., [44,45]). Each spectrum integrates into the corresponding contribution to total energy.

In Fig. 3, we show (ring-averaged) spectra $E_{\mathrm{mag}}(k_\perp)$, $E_{\mathrm{elec}}(k_\perp)$, $E_{\mathrm{bulk,sol}}(k_\perp)$, and $E_{\mathrm{bulk,comp}}(k_\perp)$ for wave vectors $k_\perp$ perpendicular to $\mathbf{B}_0$, averaged over times $11L/c \lesssim t \lesssim 22L/c$. We find that the magnetic energy and solenoidal fluid energy are in excellent equipartition across the fluid inertial range, with $E_{\mathrm{mag}}(k_\perp)$ having a scaling close to $k_\perp^{-5/3}$ while $E_{\mathrm{bulk,sol}}(k_\perp)$ has a somewhat
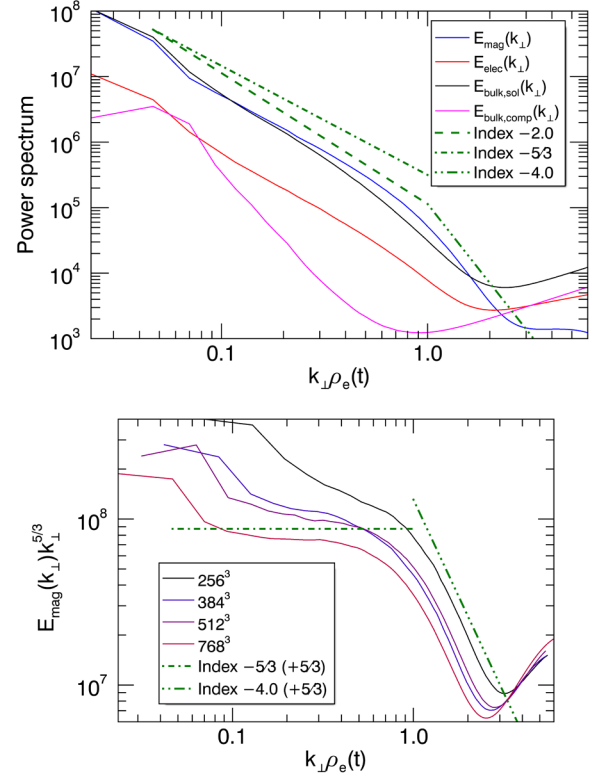

FIG. 3. Top panel: Spectra of magnetic energy $E_{\mathrm{mag}}(k_\perp)$ (blue curve), electric energy $E_{\mathrm{elec}}(k_\perp)$ (red curve), solenoidal fluid kinetic energy $E_{\mathrm{bulk,sol}}(k_\perp)$ (black curve), and compressive fluid kinetic energy $E_{\mathrm{bulk,comp}}(k_\perp)$ (magenta curve) during fully developed turbulence. Green dashed lines indicate $k_\perp^{-5/3}$ and $k_\perp^{-2}$ in the inertial range ($k_\perp \rho_e < 1$) and $k_\perp^{-4}$ in the sub-Larmor range ($k_\perp \rho_e > 1$). Bottom panel: Compensated magnetic energy spectrum $E_{\mathrm{mag}}(k_\perp)k_\perp^{5/3}$ for simulations of varying system size $L/2\pi\rho_{e0} \in \{27.2, 40.7, 54.3, 81.5\}$ and fixed $\sigma_0 = 0.25$, with $k_\perp^{-5/3}$ and $k_\perp^{-4}$ scalings (green, dashed line).

steeper scaling closer to $k_\perp^{-2}$. The electric energy and compressive fluid energy are subdominant, as expected in the subrelativistic, weakly compressible turbulence regime; in particular, $E_{\mathrm{bulk,comp}}(k_\perp)$ decreases very rapidly with $k_\perp$ (i.e., steeper than $k_\perp^{-3}$). There is a spectral break for $E_{\mathrm{mag}}(k_\perp)$ at $k_\perp \rho_e \sim 1$, in the vicinity of which there is an excess of magnetic energy over fluid energy, possibly due to the energy exchange associated with kinetic instabilities of anisotropic, nonthermal particle distributions. Beyond the spectral break, $E_{\mathrm{mag}}(k_\perp)$ steepens into a power law $k_\perp^{-4}$, implying that the cascade may continue as a kinetic cascade [46,47]. At even higher $k_\perp$, spectra flatten due to particle noise. To better characterize the inertial range, we show the compensated magnetic energy spectrum $E_{\mathrm{mag}}(k_\perp)k_\perp^{5/3}$ in the second panel in Fig. 3 and compare to simulations of smaller L/ρ_{e0} (and fixed $\sigma_0 = 0.25$). The magnetic energy spectrum approaches a scaling consistent with $k_\perp^{-5/3}$ for increasing L/ρ_{e0}, as predicted for incompressible MHD turbulence [37] and for highly relativistic MHD turbulence [48]; kinetic energy spectra steeper than $k_\perp^{-5/3}$ are
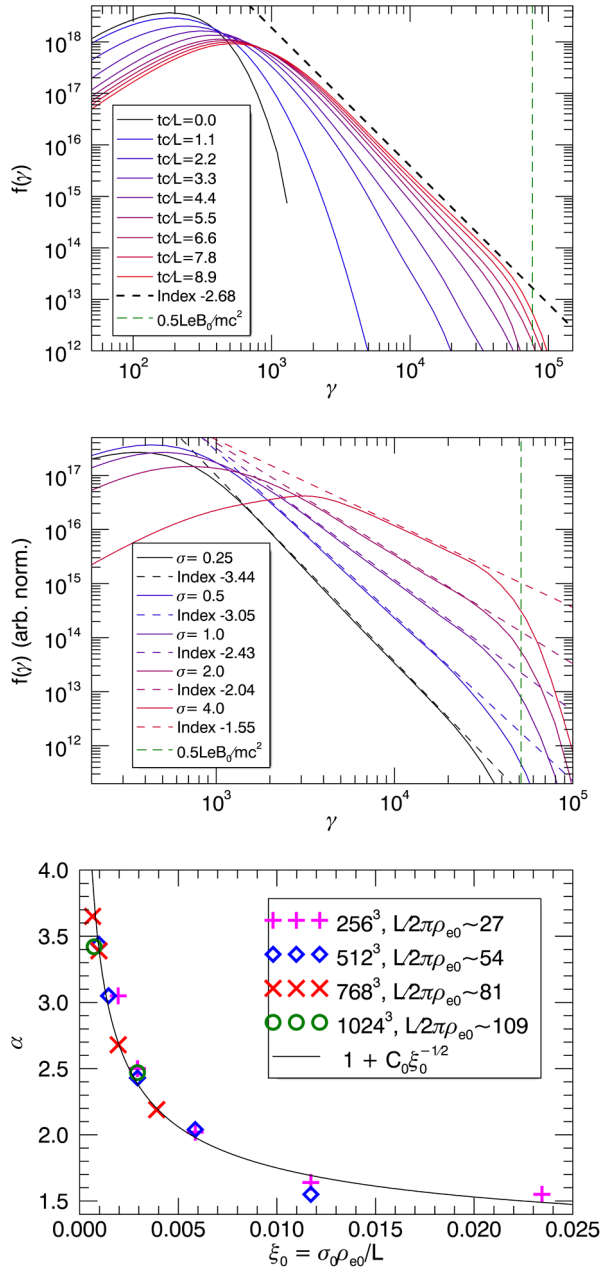
FIG. 4. Top panel: Evolution of particle energy distribution $f(\gamma)$ (where $\gamma = E/mc^2$) from the initial thermal distribution (black curve) to saturated nonthermal distribution at $t = 8.9L/c$ (red curve) (for 768^3 lattice, $\sigma_0 = 1$), along with system-size cutoff $\gamma_{\max}$ (green, dashed line) and power law $p^{-2.68}$ (black, dashed line). Middle panel: Late-time $f(\gamma)$ for $\sigma_0 \in \{1/4, 1/2, 1, 2, 4\}$ (512^3 lattice; renormalized for clarity), with respective power-law fits $p^{-\alpha}$, $\alpha \in \{3.44, 3.05, 2.43, 2.04, 1.55\}$ (dashed lines). Bottom panel: Measured α vs $\xi_0 = \sigma_0\rho_{e0}/L$, with fit $1 + C_0\xi_0^{-1/2}$ (black curve) given $C_0 = 0.075$. Data points are from 256^3 (magenta plus), 512^3 (blue diamond), 768^3 (red cross), and 1024^3 (green circle) simulations with nominal $L/2\pi\rho_{e0} \in \{27, 54, 81, 109\}$, respectively.

anticipated in both compressive [49] and relativistic [22] turbulence.

We now turn to our main result: the production of a nonthermal population of energetic particles by turbulence.

We demonstrate in Fig. 4 that the particle energy distribution converges to a power law after several dynamical times ($t \gtrsim 5L/v_{A0}$): $f(\gamma) \sim \gamma^{-\alpha}$, where $\gamma = E/mc^2$ is the particle Lorentz factor. In the second panel in Fig. 4, we show that α decreases with increasing σ_0 for a fixed system size and $\alpha < 2$ for sufficiently large σ_0. A qualitatively similar dependence of α on σ was previously found in relativistic magnetic reconnection [2,3,19]. In all of our cases, the upper cutoff for the power law is set by the system size, i.e., $\gamma_{\max} = LeB_0/2mc^2$. Since particles are unable to significantly exceed $\gamma_{\max}$, a bump forms near $\gamma_{\max}$ at late times but does not strongly influence the power law. The lower cutoff grows on the heating time scale and therefore shortens the power law for high σ_0. In addition to the σ_0 dependence, we find that the power-law distributions become steeper with increasing L/ρ_{e0}. We show the measured values of α for all of our simulations, each taken from the time with the longest fitted power-law segment, versus $\xi_0 = \sigma_0\rho_{e0}/L$ in the third panel in Fig. 4. We find that the index can be estimated, in all of our simulations, by the empirical formula $\alpha \sim 1 + C_0\xi_0^{-1/2}$, where $C_0 \approx 0.075$.

A preliminary investigation of particle acceleration mechanisms via particle tracking indicates that the acceleration process is diffusive in momentum space, consistent with second-order Fermi acceleration. Predicting the late-time power-law index α analytically is complicated, however, by the time dependence of physical parameters and the absence of a cooling mechanism or particle escape.

Conclusions.—In this Letter, we demonstrated efficient particle acceleration by driven turbulence in magnetized, collisionless, and relativistically hot plasmas for modestly large, closed domains. Our PIC simulations successfully reproduce large-scale MHD turbulence, as implied by the $k_\perp^{-5/3}$ magnetic energy spectrum. The $k_\perp^{-4}$ spectrum at sub-Larmor scales may indicate a kinetic cascade [46] and is also purportedly measured in the solar wind at scales below the electron gyroscale [50,51] [although contested (e.g., [52,53])]. The late-time particle energy distributions are robust power laws that become shallower with increasing values of $\xi = \sigma\rho_e/L$. In particular, we proposed an empirical formula for the power-law index, $\alpha \sim 1 + C_0\xi^{-1/2}$, which fits all of our simulations to a good approximation. For sufficiently high magnetization, we find that $\alpha < 2$, implying that nonthermal particles are energetically dominant and therefore kinetic physics cannot be neglected. This study provides a first step towards building a self-consistent, first-principles physical picture of driven kinetic turbulence in relativistic collisionless plasmas.

For turbulence to be a viable source of energetic particles in high-energy astrophysical systems such as pulsar wind nebulae, the late-time power-law index α must asymptotically become insensitive to the system size L (relative to ρ_e). There are no clear signs of α converging with L in our simulations, and so, if extrapolated to astrophysical system sizes ($L \gg \sigma\rho_e$ so that $\xi \ll 1$), our empirical formula

would rule out efficient turbulent particle acceleration in many astrophysical systems. However, we believe that it is reasonable to anticipate that α should approach an L-independent value for larger sizes, beyond those covered in our study. In particular, simulations of relativistic magnetic reconnection do provide evidence for an asymptotic regime in which power-law particle distributions become universal, but they approach this regime only for significantly larger systems than considered in our present work [1–3]. One may therefore expect that a longer inertial range is needed to properly resolve all of the physical processes, including instabilities, responsible for turbulent particle acceleration. In addition, since only our largest simulations exhibit a convincing inertial range, finite-size corrections to turbulence statistics may feed into the particle acceleration properties. Finally, we note that, in many astrophysical systems, additional processes such as particle escape (due to open boundaries) and radiative cooling can play an essential role in saturating the nonthermal distributions. The absence of such processes in our simulations prevents a proper steady-state distribution from being achieved and makes it nontrivial to link the indices in our dynamically evolving system to those in quasi-steady-state astrophysical systems. These important, subtle issues of convergence will await the next generation of turbulence simulations.

---

[*]zhdankin@jila.colorado.edu

[1] L. Sironi and A. Spitkovsky, Astrophys. J. Lett. **783**, L21 (2014).

[2] F. Guo, H. Li, W. Daughton, and Y.-H. Liu, Phys. Rev. Lett. **113**, 155005 (2014).

[3] G. Werner, D. Uzdensky, B. Cerutti, K. Nalewajko, and M. Begelman, Astrophys. J. Lett. **816**, L8 (2015).

[4] A. Spitkovsky, Astrophys. J. Lett. **682**, L5 (2008).

[5] L. Sironi and A. Spitkovsky, Astrophys. J. **726**, 75 (2011).

[6] A. Abdo et al., Science **331**, 739 (2011).

[7] M. Tavani et al., Science **331**, 736 (2011).

[8] J. M. Stone, E. C. Ostriker, and C. F. Gammie, Astrophys. J. Lett. **508**, L99 (1998).

[9] S. Servidio, W. H. Matthaeus, M. A. Shay, P. A. Cassak, and P. Dmitruk, Phys. Rev. Lett. **102**, 115003 (2009).

[10] G. Eyink, E. Vishniac, C. Lalescu, H. Aluie, K. Kanov, K. Bürger, R. Burns, C. Meneveau, and A. Szalay, Nature (London) **497**, 466 (2013).

[11] V. Zhdankin, D. A. Uzdensky, J. C. Perez, and S. Boldyrev, Astrophys. J. **771**, 124 (2013).

[12] E. Fermi, Phys. Rev. **75**, 1169 (1949).

[13] R. Blandford and D. Eichler, Phys. Rep. **154**, 1 (1987).

[14] J. Cho and A. Lazarian, Astrophys. J. **638**, 811 (2006).

[15] B. D. Chandran, B. Li, B. N. Rogers, E. Quataert, and K. Germaschewski, Astrophys. J. **720**, 503 (2010).

[16] V. Petrosian, Space Sci. Rev. **173**, 535 (2012).

[17] A. Lazarian, L. Vlahos, G. Kowal, H. Yan, A. Beresnyak, and E. d. G. Dal Pino, Space Sci. Rev. **173**, 557 (2012).

[18] A. Beresnyak and H. Li, Astrophys. J. **819**, 90 (2016).

[19] F. Guo, Y.-H. Liu, W. Daughton, and H. Li, Astrophys. J. **806**, 167 (2015).

[20] J. Cho, Astrophys. J. **621**, 324 (2005).

[21] J. Zrake and A. I. MacFadyen, Astrophys. J. **744**, 32 (2012).

[22] J. Zrake and A. I. MacFadyen, Astrophys. J. Lett. **763**, L12 (2012).

[23] D. Radice and L. Rezzolla, Astrophys. J. Lett. **766**, L10 (2013).

[24] J. Cho and A. Lazarian, Astrophys. J. **780**, 30 (2014).

[25] J. Zrake and W. E. East, Astrophys. J. **817**, 89 (2016).

[26] G. Kowal, E. M. de Gouveia Dal Pino, and A. Lazarian, Phys. Rev. Lett. **108**, 241102 (2012).

[27] J. W. Lynn, E. Quataert, B. D. Chandran, and I. J. Parrish, Astrophys. J. **791**, 71 (2014).

[28] K. D. Makwana, V. Zhdankin, H. Li, W. Daughton, and F. Cattaneo, Phys. Plasmas **22**, 042902 (2015).

[29] K. Nalewajko, J. Zrake, Y. Yuan, W. E. East, and R. D. Blandford, Astrophys. J. **826**, 115 (2016).

[30] Y. Yuan, K. Nalewajko, J. Zrake, W. E. East, and R. D. Blandford, Astrophys. J. **828**, 92 (2016).

[31] K. Makwana, H. Li, F. Guo, and X. Li, arXiv:1608.07829.

[32] M. Hoshino, Astrophys. J. **773**, 118 (2013).

[33] M. A. Riquelme, E. Quataert, P. Sharma, and A. Spitkovsky, Astrophys. J. **755**, 50 (2012).

[34] M. Hoshino, Phys. Rev. Lett. **114**, 061101 (2015).

[35] B. Cerutti, G. R. Werner, D. A. Uzdensky, and M. C. Begelman, Astrophys. J. **770**, 147 (2013).

[36] J. L. Synge, The Relativistic Gas (North-Holland, Amsterdam, 1957), Vol. 32.

[37] P. Goldreich and S. Sridhar, Astrophys. J. **438**, 763 (1995).

[38] J. TenBarge, G. G. Howes, W. Dorland, and G. W. Hammett, Comput. Phys. Commun. **185**, 578 (2014).

[39] J.-i. Sakai and T. Kawata, J. Phys. Soc. Jpn. **49**, 747 (1980).

[40] M. Gedalin, Phys. Rev. E **47**, 4354 (1993).

[41] Particle distributions are converged when 128 or more particles per cell are used; see Supplemental Material at http://link.aps.org/supplemental/10.1103/PhysRevLett.118 .055103 for an additional figure demonstrating this convergence.

[42] V. Zhdankin, S. Boldyrev, and D. A. Uzdensky, Phys. Plasmas **23**, 055705 (2016).

[43] M. Wan, W. Matthaeus, V. Roytershteyn, T. Parashar, P. Wu, and H. Karimabadi, Phys. Plasmas **23**, 042307 (2016).

[44] A. G. Kritsuk, M. L. Norman, P. Padoan, and R. Wagner, Astrophys. J. **665**, 416 (2007).

[45] C. Federrath, J. Roman-Duval, R. Klessen, W. Schmidt, and M.-M. Mac Low, Astron. Astrophys. **512,** A81 (2010).

[46] A. Schekochihin, S. Cowley, W. Dorland, G. Hammett, G. Howes, E. Quataert, and T. Tatsuno, Astrophys. J. Suppl. Ser. **182,** 310 (2009).

[47] K. M. Schoeffler, N. F. Loureiro, R. A. Fonseca, and L. O. Silva, Phys. Rev. Lett. **112,** 175001 (2014).

[48] C. Thompson and O. Blaes, Phys. Rev. D **57,** 3219 (1998).

[49] C. Federrath, Mon. Not. R. Astron. Soc. **436,** 1245 (2013).

[50] F. Sahraoui, M. L. Goldstein, P. Robert, and Y. V. Khotyaintsev, Phys. Rev. Lett. **102,** 231102 (2009).

[51] F. Sahraoui, S. Huang, G. Belmont, M. Goldstein, A. Rétino, P. Robert, and J. De Patoul, Astrophys. J. **777,** 15 (2013).

[52] O. Alexandrova, J. Saur, C. Lacombe, A. Mangeney, J. Mitchell, S. J. Schwartz, and P. Robert, Phys. Rev. Lett. **103,** 165003 (2009).

[53] O. Alexandrova, C. Lacombe, A. Mangeney, R. Grappin, and M. Maksimovic, Astrophys. J. **760,** 121 (2012).